Infrared water vapor continuum absorption at atmospheric temperatures

John G. Cormier, Joseph T. Hodges, and James R. Drummond

Citation: The Journal of Chemical Physics **122**, 114309 (2005); doi: 10.1063/1.1862623
View online: http://dx.doi.org/10.1063/1.1862623
View Table of Contents: http://scitation.aip.org/content/aip/journal/jcp/122/11?ver=pdfcov
Published by the AIP Publishing

Infrared water vapor continuum absorption at atmospheric temperatures

John G. Cormier[a] and Joseph T. Hodges
Chemical Sciences and Technology Laboratory, National Institute of Standards and Technology, Gaithersburg, Maryland 20899

James R. Drummond
Department of Physics, University of Toronto, 60 St. George Street, Toronto, Ontario M5S 1A7, Canada

(Received 1 December 2004; accepted 7 January 2005; published online 18 March 2005)

We have used a continuous-wave carbon dioxide laser in a single-mode realization of cavity ring-down spectroscopy to measure absorption coefficients of water vapor at 944 cm^{-1} for several temperatures in the range 270–315 K. The conventional description of water vapor infrared absorption is applied, in which the absorption is modeled in two parts consisting of local line absorption and the remaining residual absorption, which has become known as the water vapor continuum. This water vapor continuum consists of distinct water-water, water-nitrogen, and water-oxygen continua. The water-water continuum absorption coefficient is found to have a magnitude of $C_s(296\ \mathrm{K})=(1.82\pm0.02)\times10^{-22}\ \mathrm{cm^2\ molecule^{-1}\ atm^{-1}}$, and the water-nitrogen coefficient has a magnitude of $C_n(296\ \mathrm{K})=(7.3\pm0.4)\times10^{-25}\ \mathrm{cm^2\ molecule^{-1}\ atm^{-1}}$. The temperature dependences of both the water-water and the water-nitrogen continua are shown to be well represented by a model describing the expected behavior of weakly bound binary complexes. Using this model, our data yield dissociation energies of $D_e=(-15.9\pm0.3)$ kJ/mole for the water dimer and $D_e=(-3.2\pm1.7)$ kJ/mole for the water-nitrogen complex. These values are in excellent agreement with recent theoretical predictions of $D_e=-15.7$ kJ/mole (water dimer) and $D_e=-2.9$ kJ/mole (water-nitrogen complex), as well as the experimentally determined value of $D_e=(-15.3\pm2.1)$ kJ/mole for the water dimer obtained by investigators employing a thermal conductivity technique. Although there is reasonably good agreement with the magnitude of the continuum absorption coefficients, the agreement on temperature dependence is less satisfactory. While our results are suggestive of the role played by water dimers and water complexes in producing the infrared continuum, the uncertain spectroscopy of the water dimer in this spectral region prevents us from making a firm conclusion. In the meantime, empirical models of water vapor continuum absorption, essential for atmospheric radiative transfer calculations, should be refined to give better agreement with our low-uncertainty continuum absorption data. © *2005 American Institute of Physics*. [DOI: 10.1063/1.1862623]

I. INTRODUCTION

In experimental studies of the infrared absorption of water vapor, a significant excess of absorption is observed over that which could be reasonably attributed to the nearby rovibrational transitions of water vapor. This residual absorption consists of "wet continuum" and "dry continuum" components that, for historical reasons, are collectively known as the water vapor continuum.[1–5] Most observations of water vapor continuum absorption have been made in the atmospheric infrared window from 8 to 12 μm, where the continuum produces significant absorption over long atmospheric paths and thereby plays a critical role in atmospheric radiative transfer.[6–8] However, it is difficult to characterize continuum absorption from atmospheric spectra because of uncertainties in the state variables over long atmospheric paths, the effects of interfering species, and calibration issues. Meanwhile, attempts to measure water vapor continuum absorption in the laboratory using traditional techniques have suffered from low signal-to-noise ratios, instrumental baseline uncertainties, small absorption coefficients, and low sample concentrations due to the saturation vapor pressure of water. Thus, despite more than 60 years of investigation, there remains a paucity of high-quality experimental data for the mid-infrared water vapor continuum.

The generally poor quality of the existing continuum data has frustrated attempts to develop a generally accepted theoretical framework to explain the residual absorption. A possible mechanism for the water vapor continuum is the cumulative absorption of the far wings of distant yet strong water vapor transitions at atmospheric pressures. Conventional collisional line shapes (e.g., Lorentz) are based on the impact approximation, valid only for small detunings from the resonance wave number, $|\mathbf{v}-\mathbf{v}_0|\lesssim30\ \mathrm{cm^{-1}}$, and so cannot be applied to the problem of water vapor continuum absorption in which detunings from resonance of 500 cm^{-1} or more must be considered. While there has been much recent progress in the development of far wing line shapes based on the quasistatic and binary approximations,[9–15] it remains to be seen whether the accumulated far wing absorption of all

[a]Present address: Synodon Inc., 6916 Roper Road, Edmonton AB, T6B 3H9, Canada. Electronic mail: john.cormier@synodon.com

the spectral lines from neighboring absorption bands is sufficient to produce an absorption spectrum with the same magnitude and characteristics as the observed water vapor continuum.

Alternatively, it has been proposed that the infrared water vapor continuum may arise from bound pairs of water molecules (i.e., water dimers).[16,17] There is a solid thermodynamic basis to support the existence of water dimers at atmospheric conditions, although a comparison of predicted values suggests there is still considerable uncertainty in the mole fraction of water molecules that may be present in the bound state.[18] Confounding matters, theoretical dimer absorption spectra do not predict sufficient absorption in the infrared window region.[19] The evidence that is most often cited to support the dimer mechanism of continuum absorption is the apparent dependence on the square of the water vapor partial pressure in atmospheric spectra, implying that pairs of water molecules produce the absorption.[20] However, this is not a unique signature of dimer absorption since collisional broadening theories predict large self-broadening absorption cross sections for water vapor in the far wings, also producing a quadratic dependence of the absorption on the water vapor partial pressure.

Meanwhile, the formulation of water vapor continuum absorption in radiative transfer models has been identified as an important source of uncertainty in radiative transfer calculations.[6–8] A particular concern is the lack of water vapor continuum absorption data for low temperatures (i.e., below 296 K) that are typical of the Earth's atmosphere. Although attempts have been made to measure water vapor continuum absorption at low temperatures,[21–23] the data are primarily characterized by a lack of agreement. Water vapor continuum absorption coefficients in radiative transfer models are commonly represented at low temperatures by extrapolating data from higher temperatures.[24] This has the potential to produce significant errors in radiative transfer calculations, as there is evidence suggesting the continuum temperature dependence may be markedly different for the high and low temperature regimes.[25] Also problematic is the representation of the dry continuum, which consists primarily of water-nitrogen interactions but may also have a significant water-oxygen component. Our survey of the literature suggests that the water-nitrogen continuum has been rather more difficult than the water-water continuum to measure reliably, and little agreement is to be found among existing data. As a result, this important component of water vapor continuum absorption is either underestimated in radiative transfer calculations[24] or else ignored altogether.[26]

Recently, experimental continuum data have been reported in the millimeter wave region at 350 GHz spanning the temperature range 306–356 K.[27] Progress has also been reported in measuring the far-infrared continuum from 12 to 55 cm^{-1} at a temperature of 297 K.[28] To ameliorate the situation in the mid-infrared region, we have designed a temperature-controlled cavity ring-down spectroscopy (CRDS) apparatus utilizing a continuous-wave CO_2 laser source along with a high precision chilled mirror hygrometer in order to produce low-uncertainty continuum absorption data over the temperature range 270 to 315 K. Our data constrain the magnitude of the water-water and water-nitrogen continuum absorption coefficients to ±1% and ±6% respectively, and yield different insights into the temperature dependence of both components of continuum absorption.

II. EXPERIMENT

We expect that CRDS is by now sufficiently familiar that it is no longer necessary to explain in detail the underlying principles, valuable discussions of which may be found in several publications.[29–35] Briefly, a CRDS experiment operates by injecting laser energy into a high-finesse stable optical cavity (the ring-down cavity) and measuring the rate of decay of stored energy after the excitation is abruptly terminated. It is well known that stable transverse electromagnetic (TEM) field patterns, or modes, are formed inside optical cavities. By selectively exciting cavity modes with a narrowband laser source, we have observed that different cavity modes exhibit different decay rates. This probably occurs because different transverse modes sample different regions of the mirror surface, which may not have perfectly uniform effective reflectivity. To circumvent the imprecision in decay time measurements generated by multiple mode excitation, we excite only the lowest-order TEM mode (i.e., the TEM_{00} mode) of the ring-down cavity. The decay time constant τ in our single-mode CRDS experiment may be expressed as

$$\tau(\upsilon) = \frac{L}{c[(1 - R_{\text{eff}}) + k_{\text{bg}}(\upsilon)L + k(\upsilon)L]}, \tag{1}$$

where L is the cavity length, R_{eff} is the effective reflectivity of the mirrors, k_{bg} accounts for any losses (e.g., scattering) that may be due to the buffer gas [note: $k_{\text{bg}}L \ll (1-R_{\text{eff}})$ and may be treated as a constant in this experiment], and $k(\upsilon)$ is the absorption coefficient of the absorber gas at wave number υ. When the absorber gas is removed from the system, Eq. (1) reduces to

$$\tau_0(\upsilon) = \frac{L}{c[(1 - R_{\text{eff}}) + k_{\text{bg}}(\upsilon)L]}. \tag{2}$$

By algebraic manipulation of Eqs. (1) and (2), we obtain the following expression for the absorption coefficient:

$$k(\upsilon) = \frac{\tau_0(\upsilon) - \tau(\upsilon)}{c\tau_0(\upsilon)\tau(\upsilon)}. \tag{3}$$

From Eq. (3) we see that the absorption coefficient is obtained solely through measurements of decay times, quantities which are relatively easy to measure with high precision. Significantly, one is not required to measure the cavity length and mirror reflectivity to determine the absorption coefficient in CRDS. Another advantage of CRDS is that the decay time constant is insensitive to the laser amplitude fluctuations that often limits the precision of transmission-based techniques. Further, the availability of high-reflectivity mirrors enables measurements with long effective path lengths, $L_{\text{eff}} \equiv L/(1-R_{\text{eff}})$. The consequent inherent sensitivity of CRDS to weak absorption is especially important in measurements of the infrared water vapor continuum, where the small absorption cross section and saturation vapor pressure of water severely limit the absorption signal. In the present

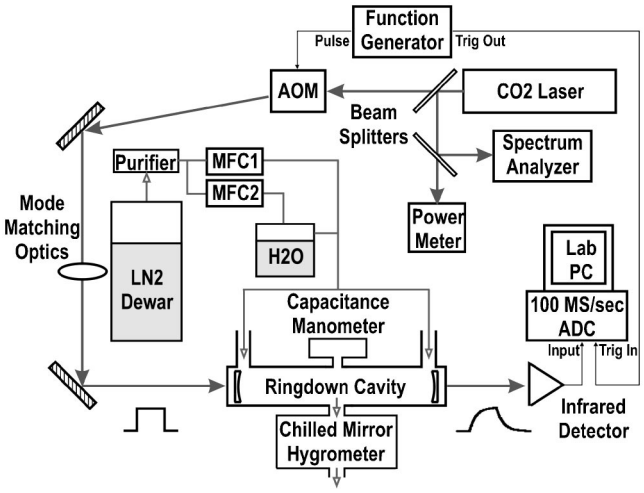

FIG. 1. Schematic layout of the infrared cavity ring-down spectroscopy experiment.

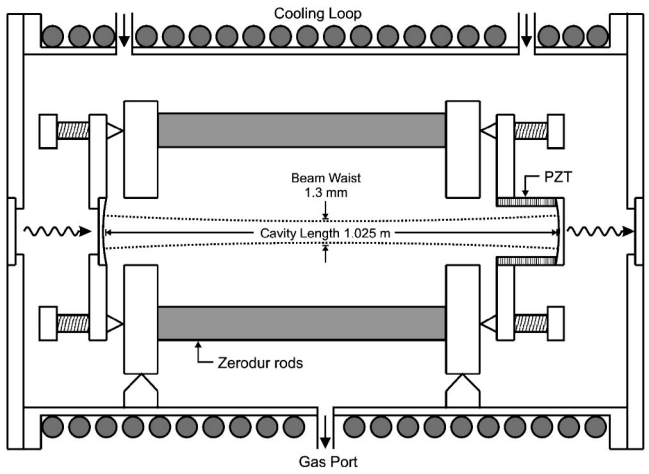

FIG. 2. Cross-section schematic view of the ring-down cell (not to scale). The length-stabilized ring-down cavity rests inside a 110 cm long, 10 cm diameter temperature-controlled cell with a gas volume of 6 l.

work, CRDS possesses yet another important advantage in that one may design a compact sample cell, enabling one to precisely control the cell temperature over a range representative of atmospheric conditions. This is in contrast to the large conventional multipass cells (i.e., White cells[36]) that have been used in several previous studies of water vapor continuum absorption.[5,37–39] Finally, our measurements demonstrate (cf., Fig. 4) that CRDS does not exhibit the instrumental baseline variations of other infrared techniques, as evidenced by the high precision and repeatability of our zero absorption (i.e., τ_0) decay time constant measurements.

Since we reported room-temperature measurements of water vapor continuum absorption,[40] we relocated the apparatus from the University of Toronto to NIST and made a number of important improvements that warrant discussion. A schematic of our CRDS apparatus is shown in Fig. 1. The laser source for these experiments is a continuous-wave CO_2 laser that is line tunable from 920 to 1090 cm^{-1} via an intracavity diffraction grating. At the output of the laser, beam splitters redirect a portion of the beam to a laser power meter and a diffraction grating spectrum analyzer to measure the CO_2 laser oscillating transition. The main portion of the laser beam is directed at an external acousto-optic modulator (AOM) operated as a first-order Bragg deflector. A function generator is used to generate electronic pulses that drive the AOM, resulting in well-defined pulses of laser radiation. The undeflected portion of the laser beam is not used in the experiment and is dissipated into a beam dump. The pulsed laser beam created by the AOM is mode matched to the TEM_{00} mode of the ring-down cavity. Infrared radiation exiting the ring-down cavity is sensed with a liquid nitrogen–cooled photovoltaic HgCdTe detector that has a rise/fall time of 20 ns. The signal from the dc-coupled output of the detector is sampled at a rate of 50 MSamples/s using a 12-bit analog-to-digital converter [Gage CS12100 (Ref. 41)]. Individual ring-down decay events, which in the present work have peak signal-to-noise ratios greater than 800:1, are stored on a computer for later analysis.

The ring-down cavity is formed using two 2.54 cm diameter concave ZnSe mirrors with 1.0 m radius of curvature and effective reflectivity $R_{\text{eff}}=0.997$ at the probe wavelength of $\lambda=10.6$ μm. The dielectric mirrors are separated a distance of 102.5 cm by a cavity assembly that is length stabilized with three zero-expansion ceramic rods having a specified linear thermal expansion coefficient $\beta \leqslant 2\times10^{-8}$ K^{-1} over the range 273–323 K. One of the mirror mounts incorporates a piezoelectric transducer to permit cavity length tuning up to 6 μm, corresponding to slightly more than one free spectral range (≈150 MHz) of the cavity. The cavity assembly rests on a three-point kinematic mount inside the cell. The ring-down cell, illustrated in Fig. 2, is constructed from a 10 cm diameter tube of electropolished 316L stainless steel that is 110 cm long and has an internal gas volume of ≈6 L. The cell is sealed at the ends with knife-edge seals and copper gaskets. Infrared radiation enters and exits the cell through antireflection coated ZnSe windows which are tilted off-normal with respect to the optical axis in order to suppress potential etaloning effects.[30,42] The pressure inside the cell was measured using a 133 kPa MKS Baratron 390HA capacitance manometer calibrated in our laboratory using a piston gauge. We consider our pressure measurements to have a standard relative uncertainty of ≈0.1%.

Our CRDS apparatus operates as a continuous-flow experiment with high-purity nitrogen as the buffer gas. The cover gas of a Dewar of liquid nitrogen is siphoned off with a two-stage stainless steel gas regulator before passing through an Aeronex model CE-500KF-I-4R inline gas purifier to reduce CO_2, H_2O, and other potential contaminants to below 1 nmol/mol.[43] To quantify the dryness of our buffer gas, we used a precision chilled-mirror hygrometer (described below) and determined the frost-point temperature of the output stream to be ⩽−90 °C, corresponding to water vapor mole fractions less than 100 nmol/mol. The flow is split into two streams using a pair of 1 L/min MKS 179A all-metal mass flow controllers. One of the streams was then passed over a body of distilled water in a temperature-controlled vessel, entraining water vapor and thereby becoming humidified. The dry and humidified gas streams are then recombined and preconditioned to the cell temperature before entering the ring-down cell. Humidified gas enters the

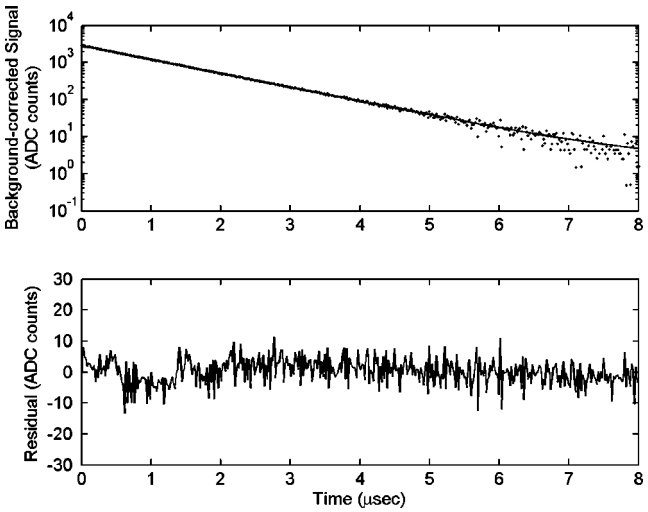

FIG. 3. Typical ring-down decay event. The background-subtracted data (ADC counts) and best fit are presented in the upper panel. The residuals are plotted in the bottom panel.

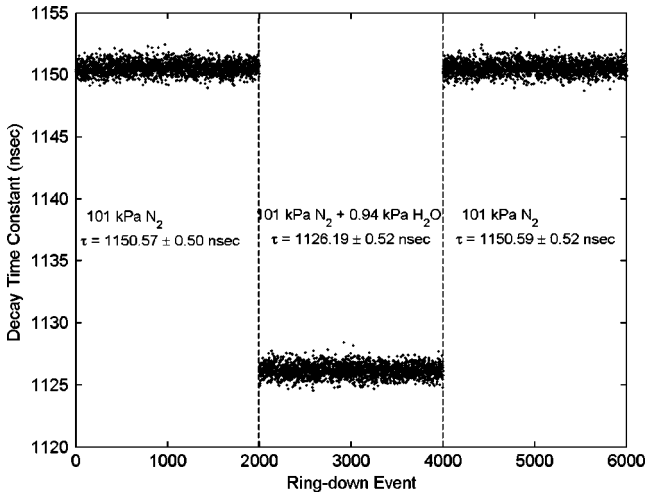

FIG. 4. Response of the infrared CRDS experiment to humidity. From left to right, the figure illustrates a sequence of three states of the system. The response of the system to each state is measured by 2000 decay events. In the first state, 101 kPa of nitrogen is flowing through the system, and we obtain the zero-absorption response corresponding to a time constant of (1150.57 ± 0.50) ns. In the second state, we introduce 0.94 kPa of water vapor to the flow, and the decay time constant drops to (1126.19 ± 0.52) ns. Finally, we restore the system to its original state of 101 kPa of nitrogen and measure a time constant of (1150.59 ± 0.52) ns.

ring-down cell via two inlet gas ports near the ends of the cell and exits the cell via a single outlet port located in the middle of the cell. Throughout the system, we use 1/4 in. electropolished 316L stainless steel tubing designed for high-purity applications, while gas line connections are made with all-metal face-seal fittings. A nominal total flow rate of 1 L/min was used throughout the measurements, and outgassing from components in the cell contributed no more than 1 μmol/mol of background humidity, as evidenced by chilled-mirror hygrometer measurements.

The humidity in the gas stream is measured at the output of the ring-down cavity using a high-precision chilled mirror hygrometer (RH Systems Model 373LX) that is traceable to NIST primary methods of humidity generation.[44,45] The temperature of the hygrometer chilled mirror is obtained from a four-wire resistance measurement of a NIST-calibrated platinum resistance thermometer (PRT), and is considered to have a standard uncertainty less than 0.1 K with a reproducibility better than ±0.05 K over the device operating range from 178 K to ambient temperatures. Our procedure is to convert the hygrometer mirror temperature into an effective water vapor partial pressure using the vapor pressure formulations $e_w(T)$ given by Wexler for liquid water[46] and ice.[47] We use Hyland's correlations for the enhancement factor of air/water vapor mixtures given by $f(T,P)$.[48,49] In these correlations, T and P are the temperature and total gas pressure, respectively, of the mixture. Wexler's correlations are modified using the appropriate conversion from the International Temperature Scale of 1968 (ITS-68) to the International Temperature Scale of 1990 (ITS-90).[50] We calculate the partial pressure of water vapor in the gas mixture using the relation $e(T)=f(T,P)\times e_w(T)$. Note that $f(T,P)$ accounts for nonideal gas effects and for small departures from ideal solution behavior (with regard to equilibrium between the gas mixture and condensed phase located at the sensing surface of the chilled-mirror hygrometer). At the conditions of this experiment, $f\approx1.004$, a factor constituting a small systematic correction to the determination of water vapor partial pressure. The improved gas handling procedures and accuracy of the hygrometer used in the present study have reduced standard relative uncertainties in water vapor partial pressure to much less than 0.5%, making this a negligible source of error in our determination of the combined uncertainty in the absorption coefficients reported below.

In order to achieve temperature control, closely spaced counterpropagating loops of 1/4 in. copper tubing were soldered along the exterior length of the ring-down cell, and a temperature-controlled chiller bath was used to circulate propylene glycol in the cooling loops. The temperature inside the cell was monitored using two NIST-calibrated PRTs. One PRT was positioned near one of the ring-down cavity mirrors and the other near the optical axis in the middle of the ring-down cavity, so that they measured as closely as possible the temperature of the gas actually interacting with the infrared radiation. To maximize the efficiency of the cooling loop and the uniformity of the cell temperature, all gas and coolant lines were carefully insulated along with the entire ring-down cell. Nevertheless, small differences in the PRT temperatures were observed that increased as the cell temperature diverged from the ambient temperature. At the lowest temperature considered in this study, 276 K, we observed a temperature difference of $\Delta T=0.5$ K between the two PRTs, while for all other temperatures the temperature difference was significantly less. We obtain the cell temperature by averaging the values from the two PRTs, and estimate that the temperature uncertainty in this study did not exceed ±0.2 K.

III. DATA ANALYSIS AND RESULTS

In this paper, we report on measurements that were obtained while the laser was operating on the 10P(20) transition at a wave number of 944.19 cm^{-1}. We trigger the AOM with pulses of duration 10 μs, while the pc-based control program archived ring-down waveforms onto the hard disk for later

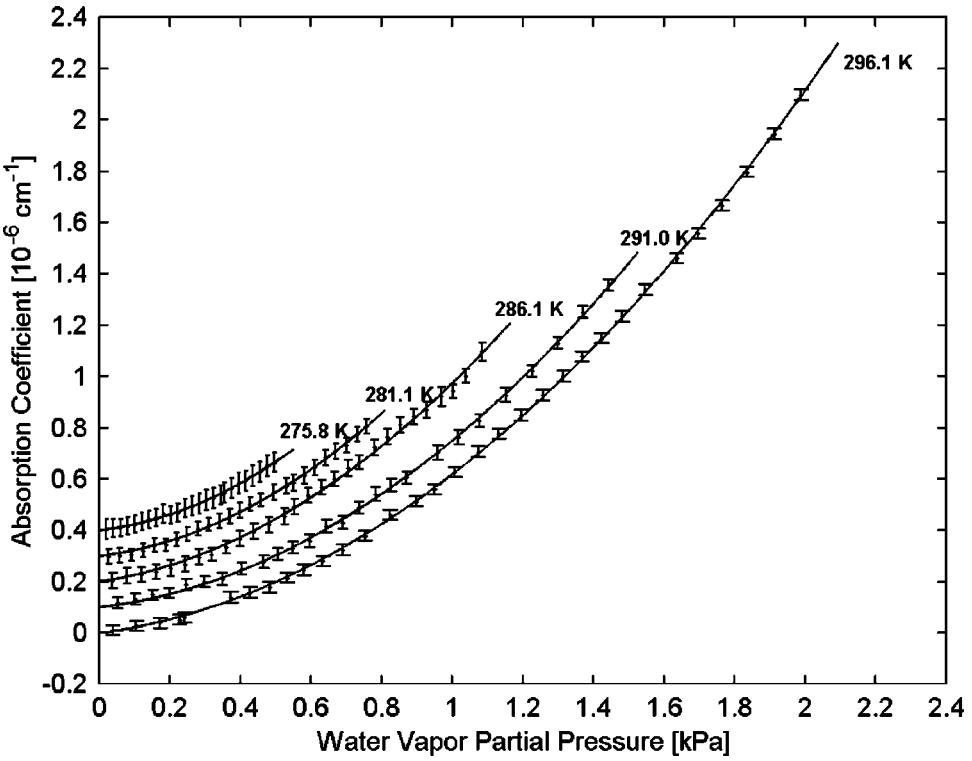

FIG. 5. Measurements of water vapor continuum absorption as a function of the water vapor partial pressure for cell temperatures from 296 K down to 276 K. The data for colder temperatures are successively offset on the vertical axis by $0.1(\times 10^{-6}\ \mathrm{cm}^{-1})$ for greater clarity. The solid curves represent the least-squares fits of the data to the empirical model given by Eq. (6).

analysis at an approximate rate of 40 Hz. In the present work, we have chosen fit windows of $\Delta t = 8\ \mu$s that begin 0.5 μs after the AOM is switched off. The effective optical path length is $L_{\mathrm{eff}} \approx 350$ m. Each decay event is fitted using an unweighted Levenberg–Marquardt least-squares minimization algorithm to the following exponential function:

$$I(t) = I_0 \exp(-t/\tau) + I_b, \tag{4}$$

where I_0, I_b, and τ are free fit parameters. A typical ring-down event is shown in Fig. 3, for which we obtain $\tau = (1149.87 \pm 0.16)$ ns. From the logarithmic plot, we see that the signal is exponential over more than three decades. The residuals to the fit, plotted in the bottom panel, are normally distributed and exhibit no discernible pattern indicative of mode-beating or other systematic effects.

In order to illustrate the response of our CRDS apparatus to the presence of water vapor in the gas stream, we present the results of a short experiment in Fig. 4. Shown left to right are three separate ensembles of decay times, each ensemble consisting of 2000 decay time measurements. The first ensemble of decay times was obtained when only 101 kPa of dry nitrogen was present in the cell for which we find a mean and standard deviation of $\tau_0 = (1150.57 \pm 0.50)$ ns. We then adjusted the mass flow controllers to introduce 0.94 kPa of water vapor to the stream and repeated the experiment, this time measuring $\tau = (1126.19 \pm 0.52)$ ns, corresponding to an absorption coefficient $k = 6.27 \times 10^{-7}$ cm^{-1}. In the final ensemble of measurements, we return the apparatus to the original conditions of 101 kPa of dry nitrogen. For this ensemble, we find $\tau_0 = (1150.59 \pm 0.52)$ ns, in excellent agreement with the original dry cell decay time constants. Interestingly, the relative imprecision of the decay time constant measurement, $\sigma_\tau/\tau = 4.4 \times 10^{-4}$, is much less than the shot-to-shot laser pulse amplitude fluctuations of about 2% that we have observed, confirming the immunity of CRDS experiments to laser amplitude fluctuations.

Water vapor absorption is treated as the sum of contributions from the local lines of water vapor and the excess absorption known as the water vapor continuum,[51]

$$k(\upsilon) = k_l(\upsilon) + k_c(\upsilon). \tag{5}$$

In practice there are two reasons why researchers have distinguished between local lines $k_l(\upsilon)$ and excess absorption $k_c(\upsilon)$. (1) Conventional line shapes (e.g., Lorentz, Voigt, etc.) are not applicable in the far wings and distinct theories can be applied in the two regimes. (2) It has been historical practice to truncate line absorption calculations at some point in the line wings to improve computational efficiency, and the excess absorption term is described separately.

In this study, we define local line absorption of water vapor as that which falls within 25 cm^{-1} of the transition wave number, and compute it using the Lorentz line shape and the spectroscopic parameters found in the HITRAN 2000 database.[52] However this truncation, although common in the literature, has no firm theoretical foundation. The formalism we have adopted to represent water vapor continuum absorption is[51]

$$k_c(\upsilon, T) = \left(\frac{1}{k_B T}\right)[C_s(\upsilon, T) \times e^2 + C_f(\upsilon, T) \times e P_f], \tag{6}$$

where k_B is the Boltzmann constant, T is the temperature, e is the water vapor partial pressure, and P_f is the foreign gas

TABLE I. Summary of measured water vapor continuum absorption coefficients as a function of cell temperature. C_s values denote the water-water continuum absorption coefficients, while C_n data refer to the water-nitrogen continuum absorption coefficients. To be consistent with the reported values of other investigators, our measurements of C_s and C_f are reported in units of $cm^2\,molecule^{-1}\,atm^{-1}$ (note: $1\ cm^2\,molecule^{-1}\,atm^{-1} = 9.869\ cm^2\,molecule^{-1}\,MPa^{-1}$). Uncertainties in the coefficients are the standard deviations of the least-squares fits of the absorption data to Eq. (6). For each value of water vapor partial pressure, an ensemble of ring-down data is collected, producing a single data point.

T(K)	Data points	C_s (10^{-22} $cm^2\,molecule^{-1}\,atm^{-1}$)	C_n (10^{-25} $cm^2\,molecule^{-1}\,atm^{-1}$)
275.8±0.3	25	2.86±0.24	8.3±1.3
281.0±0.2	25	2.50±0.10	7.6±0.9
286.1±0.1	28	2.26±0.11	8.3±1.3
291.01±0.03	26	1.99±0.04	6.6±0.6
296.06±0.03	32	1.82±0.02	7.3±0.4
301.1±0.1	36	1.62±0.02	6.3±0.4
305.2±0.2	31	1.46±0.02	6.0±0.6
310.0±0.2	29	1.37±0.02	6.6±0.5

partial pressure. In Eq. (6), k_c is in units of cm^{-1}, k_BT in atm $molecule^{-1}\,cm^3$, and P_f and e in atm. There is no well-established physical meaning for C_s and C_f, which have dimensions of area/pressure/molecule and in this paper are reported in units of $cm^2\,atm^{-1}\,molecule^{-1}$. When they are interpreted in terms of collisional broadening theories, they are often referred to as coefficients of self-broadening and foreign broadening, respectively. However, they could equally well be interpreted as the product of the absorption cross section and equilibrium constant for H_2O–H_2O and H_2O–N_2 complexes, respectively. In this paper, we have tried to adopt neutral language by referring to C_s and C_n as water-water and water-nitrogen continuum absorption coefficients, respectively.

Our low-temperature measurements of infrared continuum absorption as a function of the water vapor partial pressure are shown in Fig. 5. For greater clarity, the data are offset by increments of $0.1(\times 10^{-6}\ cm^{-1})$ on the vertical axis for each successively colder data set. Each data point in Fig. 5 corresponds to the mean value of an ensemble of 500 decay time constants, with error bars equal to the standard deviation of the ensemble. From these data, it is readily seen that the maximum observable absorption signal becomes progressively weaker as the temperature is lowered. Nevertheless, we do not appear to have reached the sensitivity limit of our apparatus, and measurements at even lower temperatures should be possible.

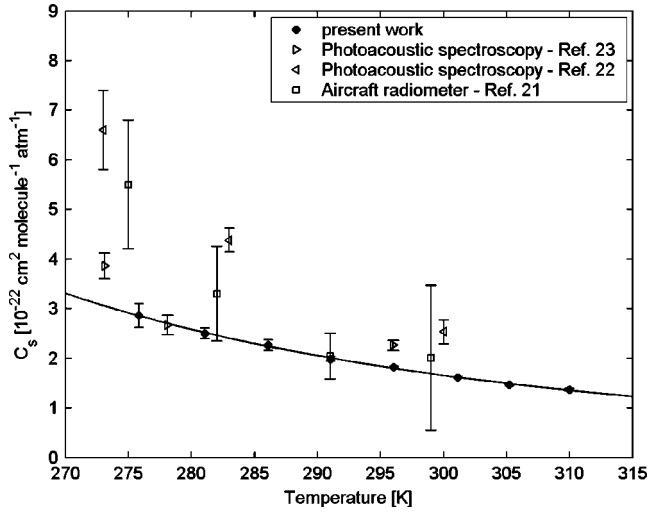

FIG. 6. The water-water continuum absorption coefficients as a function of temperature. Results from the present study are shown as solid circles. The squares are absorption coefficients derived from aircraft radiometer measurements (Ref. 21). Left- and right-facing triangles are used for the results from two previous studies in which photoacoustic spectroscopy was used (Refs. 22,23). In all cases, the error bars are those reported by the authors. Our data were fit to a power law expression to quantify the magnitude of the temperature dependence and help guide the eye.

In Fig. 6, we present water-water continuum absorption coefficients over the range of temperatures in the present study. Where available, the data of other investigators have been plotted for comparison. In one case, the data were obtained from an aircraft radiometer,[21] while the data from the other two were obtained using photoacoustic spectroscopy.[22,23] In all cases, we have represented the uncertainties as they were reported by the authors. Given the level of disagreement apparent between the data from previous studies, it seems likely the uncertainties have been underestimated. By contrast, our data, summarized in Table I, are consistent and well behaved, and seem to be adequately described by a simple model: they are reasonably well modeled by a power law expression from which we find that the temperature dependence is $-2.3\%\ K^{-1}$.

The water-nitrogen continuum absorption coefficients are plotted in Fig. 7. Our data stand alone, as we have found no comparable data sets in the literature. The uncertainties are much higher than in the case of the water-water continuum because the water-nitrogen continuum absorption coefficients are two orders of magnitude weaker. Again, our data seem to be reasonably well modeled by a power law expression, from which we find that the temperature dependence is $-0.9\%\ K^{-1}$. In Fig. 8, we plot the ratio of water-water to water-nitrogen continuum absorption coefficients, $\gamma \equiv C_s/C_n$. The value of this dimensionless parameter varies linearly from $\gamma = 200$ at 310 K to $\gamma = 350$ for our data at 276 K, with a value of $\gamma = 270 \pm 15$ at $T_0 \equiv 296$ K. Our survey of the literature suggests that values of this parameter at 296 K

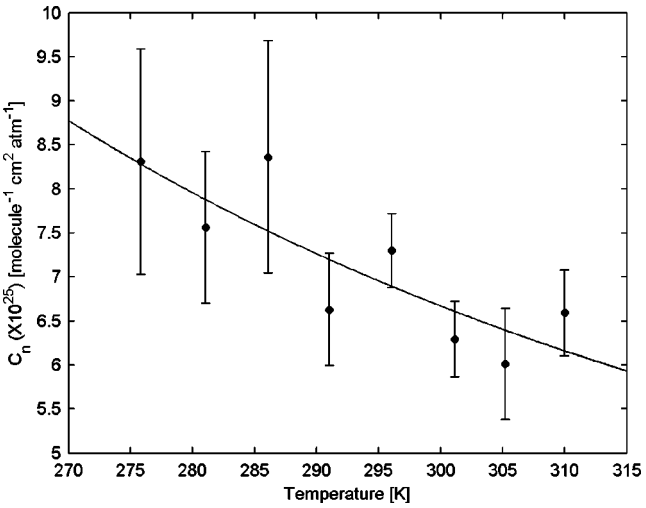

FIG. 7. The water-nitrogen continuum absorption coefficients as a function of temperature.

vary by an order of magnitude, including values of $\gamma=97$,[53] $\gamma=540$,[22] and $\gamma=710$,[23] all of which were obtained using photoacoustic spectroscopy. Finally, our results appear to be in exact agreement with the $\gamma=270$ value reported by Peterson *et al.*,[38] also obtained using photoacoustic spectroscopy, but that is probably a coincidence.

Because there is only an incomplete body of experimental data, atmospheric scientists have had to implement empirical models of continuum absorption in radiative transfer algorithms. Perhaps the most widely used of these has been the "CKD 2.4" empirical model of continuum absorption.[54] The CKD 2.4 values of the self- and foreign-broadened continuum coefficients at $v=944\ \mathrm{cm}^{-1}$ and $T=296$ K are $C_s(\mathrm{CKD\ 2.4})=2.33\times10^{-22}\ \mathrm{cm}^2\ \mathrm{molecule}^{-1}\ \mathrm{atm}^{-1}$ and $C_f(\mathrm{CKD\ 2.4})=4.08\times10^{-27}\ \mathrm{cm}^2\ \mathrm{molecule}^{-1}\ \mathrm{atm}^{-1}$, producing a value of $\gamma=57\,100$ that is 210 times larger than our value. In the recently revised CKD model, dubbed "MT_CKD," the continuum coefficients are $C_s(\mathrm{MT\_CKD})=2.21\times10^{-22}\ \mathrm{cm}^2\ \mathrm{molecule}^{-1}\ \mathrm{atm}^{-1}$ and $C_f(\mathrm{MT\_CKD})=8.69\times10^{-26}\ \mathrm{cm}^2\ \mathrm{molecule}^{-1}\ \mathrm{atm}^{-1}$, producing a value of $\gamma=2540$ that is almost 10 times larger than our measured value.[55] Unfortunately, these comparisons suggest that there may be significant errors in the modeling of continuum absorption in atmospheric radiative transfer calculations due to the use of empirical models such as the CKD model.[6–8]

IV. DISCUSSION

The nature and origin of the water vapor continuum has been the subject of considerable speculation and controversy since the existence of this continuous absorption spectrum was first proposed in 1938.[1] Although a variety of hypotheses have been advanced, most of the attention and development has centered around the far wing and the water dimer hypotheses. To test the consistency of our infrared continuum measurements with these two prevailing hypotheses, we compare the measured temperature dependence of C_s and C_n to their respective model temperature dependences.

The functional form of the temperature dependences of the water-water complex (i.e., water dimer) and the water-nitrogen complex is obtained from a recently proposed model of weakly bound binary complexes.[56] This model predicts that the temperature dependence of the infrared continuum absorption coefficients as defined by our Eq. (6) should follow the form:

$$C_s(\nu,T)=C_s^0(\nu)\times\left(\frac{T_0}{T}\right)^{n-1}\left[\frac{\exp(-D_e/k_BT)-\left(1-\frac{D_e}{k_BT}\right)}{\exp(-D_e/k_BT_0)-\left(1-\frac{D_e}{k_BT_0}\right)}\right],$$

$$C_n(\nu,T)=C_n^0(\nu)\times\left(\frac{T_0}{T}\right)^{n-1}\left[\frac{\exp(-D_e^*/k_BT)-\left(1-\frac{D_e^*}{k_BT}\right)}{\exp(-D_e^*/k_BT_0)-\left(1-\frac{D_e^*}{k_BT_0}\right)}\right], \tag{7}$$

where D_e and D_e^* are the dissociation energies of the water dimer and water-nitrogen complex, respectively. Note that a slight typographical error in the definition of the temperature exponent, n, appears on p. 32 of the above-cited work, which should read $n=5/2-(m+\chi)$. In the present work, we have chosen values of n corresponding to the harmonic oscillator approximation, i.e., $n=\frac{1}{2}$ for water-water and $n=1$ for water-nitrogen.

Meanwhile, the continuum absorption coefficients derived from the far wing line shape theory must be determined numerically, which would suggest there is no simple analytical form that could be used to represent the temperature dependence. Nevertheless, we have found that to an excellent approximation, the temperature dependence of the far wing continuum absorption coefficients can be modeled using the following exponential form:[26]

$$C_s(\nu,T)=C_s^o(\nu)\exp\left[-T_e\left(\frac{1}{T}-\frac{1}{T_0}\right)\right],$$

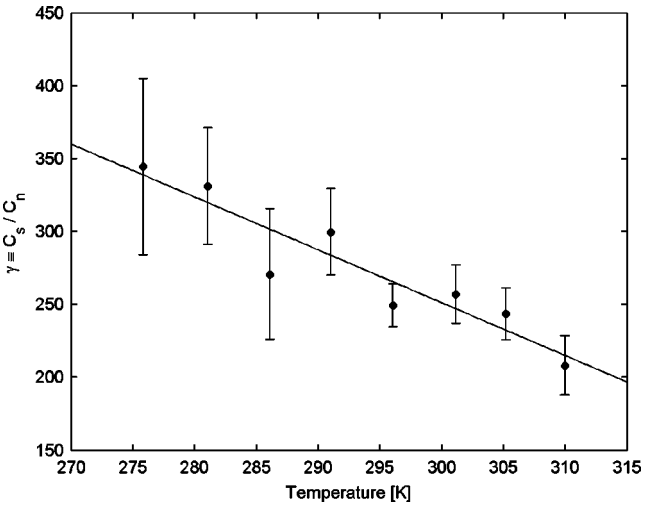

FIG. 8. Ratio of the water-water and water-nitrogen continuum absorption coefficients as a function of temperature.

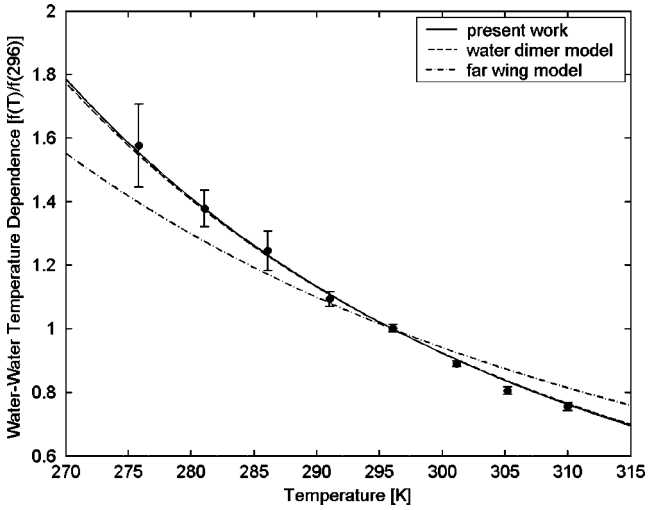

FIG. 9. The temperature dependence of the water-water continuum, normalized to 296 K. Experimental data from the present work are represented with appropriate error bars and a solid line best fit. The dashed line represents the weakly bound complex model, using the value $n=0.5$ (harmonic oscillator) and $D_e=-15.7$ kJ/mole, while the dotted line represents continuum absorption coefficients derived from the far wing theory.

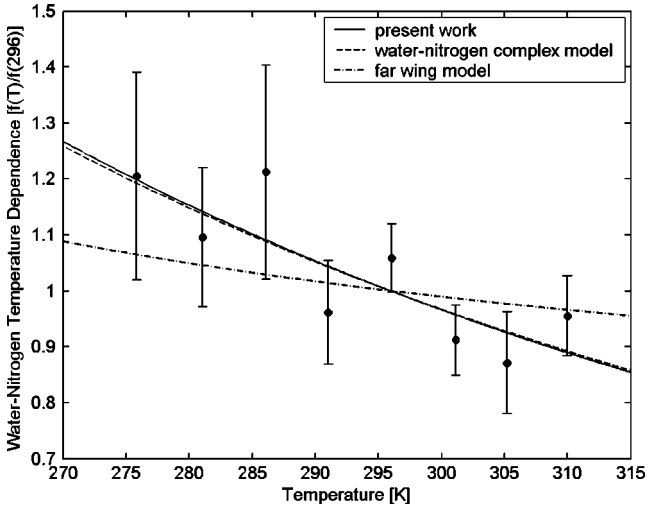

FIG. 10. The temperature dependence of the water-nitrogen continuum, normalized to 296 K. Experimental data from the present work are represented with appropriate error bars and a solid line best fit. The dashed line represents the weakly bound complex model, using the value $n=1$ (harmonic oscillator) and $D_e^*=-2.9$ kJ/mole, while the dotted line represents continuum absorption coefficients derived from the far wing theory.

$$C_n(\nu,T)=C_n^o(\nu)\exp\left[-T_e^*\left(\frac{1}{T}-\frac{1}{T_0}\right)\right], \tag{8}$$

where T_e and T_e^* are characteristic temperatures of the exponential temperature dependence for self-broadening and nitrogen broadening, respectively. From our least squares fits to the Ma and Tipping far wing continuum absorption coefficients for water-water[15] and water-nitrogen,[14] we obtain $T_e=1350$ K and $T_e^*=300$ K.

Our water-water continuum data, normalized to 296 K, is presented in Fig. 9 along with curves representing the water dimer temperature dependence (dashed line) and the far wing temperature dependence (dotted line). To represent the dissociation energy of the water dimer in Eq. (7), we used the value of $D_e=-15.7$ kJ/mole that was recently obtained from the VRT(ASP-W)III water dimer intermolecular potential energy surface.[18] In Fig. 10, we present the water-nitrogen continuum data (again, normalized to 296 K), along with curves representing the water dimer temperature dependence (dashed line) and the far wing temperature dependence (dotted line). For this case, we represent the dissociation energy of the water-nitrogen complex using the value of $D_e^*=-2.9$ kJ/mole derived from *ab initio* calculations and tuned with experimental rotational and quadrupole coupling constants.[57] When our data are fitted to the weakly bound complex model, we obtain dissociation energies of $D_e=(-15.9\pm0.3)$ kJ/mole for the water dimer, and $D_e^*=(-3.2\pm1.7)$ kJ/mole for the water-nitrogen complex.

What is most striking to us, indeed rather surprising, is the extraordinary agreement that is demonstrated between our water-water and the water-nitrogen data sets and the temperature dependence of the weakly bound binary complex model. Based on the observed temperature dependence and the clear quadratic dependence on the water vapor partial pressure demonstrated in the data presented in Fig. 5, it is tempting to conclude that the infrared water vapor continuum results from the formation of water dimers and water-nitrogen complexes. Although such a conclusion appears to have been recently reached by investigators with less convincing data at their disposal,[20] we hesitate to concur. First, theoretical calculations of far wing continuum absorption may be significantly determined by the choice of intermolecular potential, and given the calculational challenges it is unclear whether the most accurate potentials have been employed. Second, there are no reliable cross sections for water dimer absorption in the 1000 cm^{-1} spectral region, making it difficult to validate the predicted magnitude of dimer absorption. Nevertheless, it must be said that the present results are not incompatible with the notion of water dimer and water-nitrogen complex absorption in the atmosphere, and moreover we believe that the present results are sufficiently compelling to warrant a closer examination of continuum absorption in this and other regions of the spectrum.

We conclude this section with some thoughts on the performance of the apparatus. From the data, we estimate the minimum detectable absorption coefficient of our CRDS apparatus to be $k_{\min}=1.2\times10^{-8}$ cm^{-1}. We have not found in the literature accounts of any spectroscopic experiments operating in the mid-infrared region with better sensitivity. Although photoacoustic spectroscopy (PAS) has the potential to be a sensitive technique,[58] experimentalists have found that the real detection limits of PAS are usually two orders of magnitude above the theoretical detection limits, i.e., above 10^{-7} cm^{-1}.[23] In addition to sensitivity-limiting acoustical background noise, the accuracy of PAS data may be compromised by systematic effects such as calibration uncertainties. Surveys of the published values of ethylene absorption coefficients used for PAS calibration have revealed discrepancies on the order of ±10%.[23,59]

By comparison, the experiment we have presently described, based on the principles of CRDS and a flowing gas methodology, does not require the use of a calibration gas.

Low-uncertainty water vapor absorption coefficients are directly obtained from measurements of decay time constants when water vapor is added and then removed from the gas stream. Meanwhile, the compact design allows us to maintain good control over the gas conditions in the cell, and to adjust the temperature over the range 270–315 K. Equally important, the flowing gas methodology permits us to make a rapid and accurate measurement of humidity using a high precision chilled-mirror hygrometer. The combination of relatively low-uncertainty measurements of both the absorption coefficient and the water vapor partial pressure in the system has produced a low-uncertainty water vapor continuum data set that could be used to validate theoretical models of continuum absorption.

Although chilled-mirror hygrometers are considered to be the most accurate method of humidity measurement, a potential source of uncertainty arises for mirror temperatures in the range between 0 °C and ≈−20 °C. Because either dew or frost may form on the mirror surface in this temperature range, this can lead to errors as high as 15% in the reporting of humidity in the gas stream. To avoid this, we took advantage of the "force frost" feature of the RH Systems hygrometer, which quickly drives the mirror temperature down to −40 °C forcing the formation of a frost layer before the instrument reacquires the frost point. Additionally, experience has taught us to approach humidities in this range from the low side, further ensuring that a frost layer was present on the mirror surface.

We believe that improvements in our procedures and instrumentation account for most of the discrepancy between our present results and those from our previous study of water vapor continuum absorption,[40] in which we found $C_s = (2.02 \pm 0.13) \times 10^{-22}$ cm^2 molecule^{-1} atm^{-1} at $T = 294$ K. In our earlier work, we employed a chilled-mirror hygrometer that could not discriminate between dew and frost on the mirror. More importantly, we have since discovered that in our earlier work a small systematic error was introduced in the reported water vapor partial pressures because we failed to properly account for the difference in total pressure between the hygrometer chamber and the ring-down cell under gas flow conditions. Even though the corrections to our previously measured water vapor partial pressures increase their values by less than 3%, the result is nevertheless a significant reduction in the refitted value of the water-water continuum absorption coefficient to $C_s = (1.88 \pm 0.13) \times 10^{-22}$ cm^2 molecule^{-1} atm^{-1}, i.e., within experimental uncertainties of our present result of $C_s = (1.82 \pm 0.02) \times 10^{-22}$ cm^2 molecule^{-1} atm^{-1}. We therefore conclude that small errors in the measurement of humidity significantly influence the determination of the water-water continuum absorption coefficients. In fact, small errors in the measurement of humidity might account for the major part of the ±20%–30% scatter in observed continuum coefficients.[23,60]

Finally, we note that a potentially significant model-dependent error arises from the fact that the empirical definition of continuum absorption is inextricably linked to the definition of local lines. By inspection of Eq. (5), it is apparent that systematic errors in the local line parameters could produce corresponding systematic errors in the continuum absorption coefficients. By choosing to measure the continuum at a wavelength where the contribution from local lines is very small, uncertainties arising from errors in the spectroscopic database should be minimized. To test this assumption, we reanalyzed our data after applying a shift of 20% in the calculated local line absorption, representative of line strength and broadening parameter uncertainties in this spectral region.[61] We find that the water-water continuum absorption coefficients were unaffected, although the water-nitrogen continuum coefficients were shifted by 5%. Given the uncertainties of ±10% in our water-nitrogen continuum absorption coefficients (Table I), it seems unlikely that future revisions to the spectroscopic line databases would cause the C_n values to shift beyond their present uncertainties.

V. SUMMARY

We have developed a gas flow CRDS apparatus that permits water vapor continuum absorption to be measured with low uncertainty in the important 900–1100 cm^{-1} infrared window region. This apparatus was developed at the University of Toronto and subsequently improved at NIST where the present measurements were performed. The sensitivity of the apparatus is equivalent to a minimum detectable absorption coefficient $k_{\min} = 4.1 \times 10^{-10}$ cm^{-1} Hz$^{-1/2}$. In the present work, we report on measurements made at 944 cm^{-1} over the temperature range 270–315 K, temperatures that are representative of nearly all atmospheric conditions of interest. Our measurements of water-water continuum absorption constrain the magnitude to an uncertainty of ±1% near room temperature, confirm the existence of a water-nitrogen continuum and constrain the water-nitrogen continuum absorption coefficients to an uncertainty of ±6%.

For atmospheric modeling, the water-water continuum and the water-nitrogen continuum are probably the most important of such interactions, although the possibility of a water-oxygen continuum that is significantly different from these should be investigated further.[62] Given the advances reported herein in measurement capabilities, we think it is now possible to quantify the effect of different gases on continuum absorption with reasonable accuracy.

The temperature dependence of the water-water and water-nitrogen continua are shown to be in excellent agreement with the weakly bound binary complex model. This behavior, along with the quadratic partial pressure dependence, is strongly suggestive of the important role played by atmospheric water dimers and water complexes. We are prevented from reaching a firm conclusion because there are large uncertainties in the spectroscopy of water dimers near 1000 cm^{-1}, and also because we think that further refinements to the far wing may produce better agreement than is presently demonstrated. Nevertheless, it is hoped that our results will stimulate further theoretical and experimental advances into the nature and origins of continuum absorption.

ACKNOWLEDGMENTS

J.G.C. would like to acknowledge the United States National Research Council Research Associateship Program for the Postdoctoral Research Fellowship Award that made this

collaboration possible. Important additional financial support for this project was provided by the COMDEV/BOMEM/AES/CSA/NSERC University of Toronto Industrial Research Chair in Remote Sounding From Space. The authors are also grateful for the valuable technical assistance of Jeff Anderson, Wyatt Miller, and Greg Scace at NIST. The many helpful comments of J. Patrick Looney and Roman Ciurylo in the preparation of this manuscript are also gratefully acknowledged.

[1]W. M. Elsasser, Phys. Rev. **53**, 768 (1938).
[2]A. Adel, Astrophys. J. **89**, 1 (1939).
[3]W. T. Roach and R. M. Goody, Q. J. R. Meteorol. Soc. **84**, 319 (1958).
[4]K. Bignell, F. Saiedy, and P. A. Sheppard, J. Opt. Soc. Am. **53**, 466 (1963).
[5]K. J. Bignell, Q. J. R. Meteorol. Soc. **96**, 390 (1970).
[6]A. Slingo and R. C. Winderspin, Q. J. R. Meteorol. Soc. **112**, 371 (1986).
[7]F. M. Luther, R. G. Ellingson, Y. Fouquart, S. Fels, N. A. Scott, and W. J. Wiscombe, Bull. Am. Meteorol. Soc. **69**, 40 (1988).
[8]W. L. Ridgway, Harshvarshan, and A. Arking, J. Geophys. Res. **D96**, 8969 (1991).
[9]P. W. Rosenkranz, J. Chem. Phys. **83**, 6139 (1985).
[10]P. W. Rosenkranz, J. Chem. Phys. **87**, 163 (1987).
[11]Q. Ma and R. H. Tipping, J. Chem. Phys. **95**, 6290 (1991).
[12]R. H. Tipping and Q. Ma, Atmos. Res. **36**, 69 (1995).
[13]Q. Ma and R. H. Tipping, J. Chem. Phys. **111**, 5909 (1999).
[14]Q. Ma and R. H. Tipping, J. Chem. Phys. **112**, 574 (2000).
[15]Q. Ma and R. H. Tipping, J. Chem. Phys. **116**, 4102 (2002).
[16]S. S. Penner and P. Varanasi, J. Quant. Spectrosc. Radiat. Transf. **7**, 687 (1967).
[17]P. Varanasi, S. Chou, and S. S. Penner, J. Quant. Spectrosc. Radiat. Transf. **8**, 1537 (1968).
[18]N. Goldman, C. Leforestier, and R. J. Saykally, J. Phys. Chem. A **108**, 787 (2004).
[19]H. C. W. Tso, D. J. W. Geldart, and P. Chylek, J. Chem. Phys. **108**, 5319 (1998).
[20]K. Pfeilsticker, A. Lotter, C. Peters, and H. Bösch, Science **300**, 2078 (2003).
[21]M. T. Coffey, Q. J. R. Meteorol. Soc. **103**, 685 (1977).
[22]G. L. Loper, M. A. O'Neill, and J. A. Gelbwachs, Appl. Opt. **22**, 3701 (1983).
[23]J. Hinderling, M. W. Sigrist, and F. K. Kneubühl, Infrared Phys. **27**, 63 (1987).
[24]S. A. Clough, M. J. Iacono, and J. L. Moncet, J. Geophys. Res. **D97**, 15761 (1992).
[25]G. P. Montgomery, Appl. Opt. **17**, 2299 (1978).
[26]R. E. Roberts, J. E. A. Selby, and L. M. Biberman, Appl. Opt. **15**, 2085 (1976).
[27]T. Kuhn, A. Bauer, M. Godon, S. Bühler, and K. Künzi, J. Quant. Spectrosc. Radiat. Transf. **74**, 545 (2002).
[28]V. B. Podobedov, D. F. Plusquellic, and G. T. Fraser, J. Quant. Spectrosc. Radiat. Transf. **91**, 287 (2005).
[29]A. O'Keefe and D. A. G. Deacon, Rev. Sci. Instrum. **59**, 2544 (1988).
[30]D. Romanini and K. K. Lehmann, J. Chem. Phys. **99**, 6287 (1993).
[31]K. K. Lehmann and D. Romanini, J. Chem. Phys. **105**, 10263 (1996).
[32]J. T. Hodges, J. P. Looney, and R. D. van Zee, J. Chem. Phys. **105**, 10278 (1996).
[33]J. P. Looney, J. T. Hodges, and R. D. van Zee, in *Cavity-Ringdown Spectroscopy: An Ultratrace-Absorption Measurement Technique*, edited by K. W. Busch and M. A. Busch (American Chemical Society, Washington, DC, 1999), p. 93.
[34]J. G. Cormier, J. T. Hodges, and J. R. Drummond, in *Spectral Line Shapes*, edited by C. A. Back, AIP Conf. Proc. No 645 (AIP, New York, 2002), Vol. 12, p. 401.
[35]J. T. Hodges, H. P. Layer, W. W. Miller, and G. E. Scace, Rev. Sci. Instrum. **75**, 849 (2004).
[36]J. U. White, J. Opt. Soc. Am. **32**, 285 (1942).
[37]J. H. McCoy, D. B. Rensch, and R. K. Long, Appl. Opt. **8**, 1471 (1969).
[38]J. C. Peterson, M. E. Thomas, R. J. Nordstrom, E. K. Damon, and R. K. Long, Appl. Opt. **18**, 834 (1979).
[39]D. E. Burch and R. L. Alt, AFGL Report No. AFGL-TR-84-0128, (Hanscom AFB, Bedford, MA, 1984).
[40]J. G. Cormier, R. Ciurylo, and J. R. Drummond, J. Chem. Phys. **116**, 1030 (2002).
[41]Manufacturers and product names are listed solely for completeness. These specific endnotes neither constitute an endorsement of the products nor imply that similar products from other companies would be less suitable.
[42]J. B. Dudek, P. B. Tarsa, A. Velasquez, M. Wladyslawski, P. Rabinowitz, and K. K. Lehmann, Anal. Chem. **75**, 4599 (2003).
[43]See www.aeronex.com
[44]G. E. Scace and J. T. Hodges, in *Proceedings of the Eighth International Symposium on Temperature and Thermal Measurements in Industry and Science (TEMPMEKO 2001)*, edited by B. Fellmuth *et al.* (VDE, Berlin, 2002), p. 597.
[45]S. Hasegawa and J. W. Little, J. Res. Natl. Bur. Stand., Sect. A **81A**, 81 (1977).
[46]A. Wexler, J. Res. Natl. Bur. Stand., Sect. A **80A**, 775 (1976).
[47]A. Wexler, J. Res. Natl. Bur. Stand., Sect. A **81A**, 5 (1977).
[48]R. W. Hyland, J. Res. Natl. Bur. Stand., Sect. A **79A**, 551 (1975).
[49]R. W. Hyland and A. Wexler, ASHRAE Trans. **89**, 520 (1983).
[50]H. Preston-Thomas and T. J. Quinn, *Techniques for Approximating the International Temperature Scale of 1990*, 1st ed. (Bureau International des Poids et Mésures, Pavillon de Breteuil, Sèvres, 1990), Appendix A.
[51]P. Varanasi and S. Chudamani, J. Quant. Spectrosc. Radiat. Transf. **38**, 407 (1987).
[52]L. S. Rothman, A. Barbe, D. C. Benner *et al.*, J. Quant. Spectrosc. Radiat. Transf. **82**, 5 (2003).
[53]M. S. Shumate, R. T. Menzies, J. S. Margolis, and L.-G. Rosengren, Appl. Opt. **15**, 2480 (1976).
[54]S. A. Clough, F. X. Kneizys, and R. W. Davies, Atmos. Res. **23**, 229 (1989).
[55]See www.aer.com
[56]A. A. Vigasin, J. Quant. Spectrosc. Radiat. Transf. **64**, 25 (2000).
[57]P. Sandler, J. oh Jung, M. M. Szczesniak, and V. Buch, J. Chem. Phys. **101**, 1378 (1994).
[58]L. B. Kreuzer, J. Appl. Phys. **42**, 2934 (1971).
[59]J. S. Ryan, M. H. Hubert, and R. A. Crane, Appl. Opt. **22**, 711 (1983).
[60]W. B. Grant, Appl. Opt. **29**, 451 (1990).
[61]L. S. Rothman, C. P. Rinsland, A. Goldman *et al.*, J. Quant. Spectrosc. Radiat. Transf. **60**, 665 (1998).
[62]R. J. Nordstrom, M. E. Thomas, J. C. Peterson, E. K. Damon, and R. K. Long, Appl. Opt. **17**, 2724 (1978).